Propagation of a Penny-Shaped Hydraulic Fracture Parallel to a Free-Surface, with Application to Inducing Rock Mass Caving for Mining

Xi Zhang
CSIRO Petroleum, PO Box 3000, Glen Waverley, VIC, Australia

Emmanuel Detournay
Department of Civil Engineering, University of Minnesota, Minneapolis, MN, USA

Rob Jeffrey
CSIRO Petroleum, PO Box 3000, Glen Waverley, VIC, Australia

ABSTRACT: In this paper, the problem of a penny-shaped hydraulic fracture propagating parallel to the free-surface of an elastic half-space is studied. The fracture is driven by an incompressible Newtonian fluid injected at a constant rate. The flow of viscous fluid in the fracture is governed by the lubrication equation, while the crack opening and the fluid pressure are related by singular integral equations. We construct two asymptotic solutions based on the assumption that the energy expended in the creation of new fracture surfaces is either small or large compared to the energy dissipated in viscous flow. One important outcome of the analysis is to show that the asymptotic solutions, when properly scaled, depend only on the dimensionless parameter $\mathcal{R}$, the ratio of the fracture radius over the distance from the fracture to the free-surface. The scaled solutions can thus be tabulated and the dependence of the solution on time can be retrieved for specific parameters, through simple scaling and by solving an implicit equation.

1 INTRODUCTION

Hydraulic fracturing is the most common method used to stimulate production from gas and oil wells. The fractures are propagated from the well to stimulate reservoirs that are typically located 500 to several thousand meters below the surface. Hydraulic fracture growth at these depths is not affected by the surface of the earth, although surface deformation (tilt) is sometimes measured to infer fracture orientation and size.

Although most fractures arising from hydraulic fracture treatments can be conceptualized as propagating within an infinite space, there are specific cases where the influence of a free-surface on the fracture growth becomes significant or even dominant. Hydraulic fracturing has recently been used in mining to induce and control the timing of rock caving event, see Jeffrey & Mills (2000). The work contained in this paper is motivated by hydraulic fracturig used underground at Moonee Colliery to control the timing of roof-rock caving events. At Moonee, a massive conglomerate roof rock does not cave behind the longwall face in a predictable way and, when it does cave, produces a strong windblast in the nearby mine workings. Moonee has adopted hydraulic fracturing as a way to induce the conglomerate to cave in a controlled time period. The hydraulic fractures are formed at the end of 8 m long vertical holes drilled up into the conglomerate, as shown in Fig. 1. The treatments produce more or less axisymmetric horizontal fractures that grow parallel to and strongly affected by the free surface. Fracture behaviors are characterized by a ratio of the fracture radius over the distance from the free surface which can reach order 1 or more. (See, also, Pollard & Hozlhausen (1979) for a granite quarry example.)

The problem of predicting the fluid pressure, opening and size of the fracture given the injection rate, fluid rheology, and rock properties has attracted an extraordinary number of contributions since the 1950s. This intense research activity has contributed to the formulation of a variety of models that emphasize either the design of a hydraulic fracturing treatment, or the exact solution of the coupled fluid-solid problem with simple fracture geometry (Savitski & Detournay 2000). However, the influence of a free-surface on the propagation of a fluid-driven fracture has not yet been addressed, except approximately (Jeffrey & Settari, 2000) and by a few contributions dealing with the problem of a uniformly pressurized fracture(Wang et al. 1994).

We analyze the problem of a penny-shaped hydraulic fracture propagating at a constant distance H from the free-surface of an elastic half-space, see Fig. 1. The fracture is driven by injection of an incompressible, Newtonian fluid at a constant volumetric rate Q_o from a point source. (The borehole sketched in Fig. 1 to inject fluid is assumed to have zero radius in the subsequent analysis.) The half-space is prestressed with a lateral uniform compressive stress $\sigma_r = -\sigma_o$ and an axial stress $\sigma_z = \alpha z$, where $\alpha = 0$ or $\pm\gamma$ – with γ denoting the unit weight of the material – depending on the orientation of the half-space and whether or not gravity needs to be accounted for in the analysis.

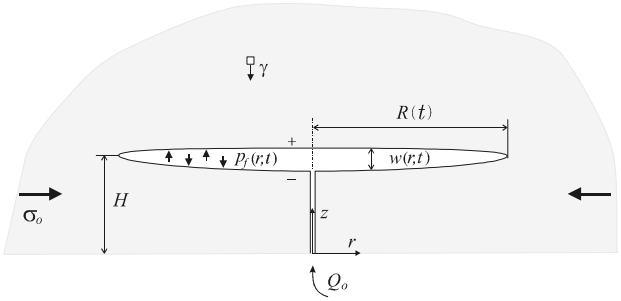

Figure 1: Penny-shaped hydraulic fracture propagating parallel to the free-surface of an elastic half-space

The objective of this paper is to present solutions for predicting the evolution of the fracture radius R with time, as well as the dependence of the opening w, and net pressure $p = p_f \pm \alpha H$ upon the radial distance r and time t. In particular, we are interested in mapping the dependence of the solution on the injection rate Q_o and on the three material parameters μ', E', K' defined as

$$\mu' = 12\mu,\ E' = \frac{E}{1-\nu^2},\ K' = 4\left(\frac{2}{\pi}\right)^{1/2} K_{Ic} \quad (1)$$

where μ is the fluid viscosity, E and ν the rock Young's modulus and Poisson's ratio, and K_{Ic} the rock fracture toughness. For the sake of convenience, μ', E', and K' will simply be referred to as viscosity, elastic modulus, and toughness, respectively.

In this paper, we only consider the problem of obtaining solutions for the two limiting cases of viscosity- and toughness-dominated fracture growth. In the viscosity-dominated regime, the energy expended in the creation of new fracture surfaces in the rock is small compared to the energy dissipated in viscous flow; in the toughness-dominated regime, the viscous dissipation is small compared to the energy dissipated at the crack tip (Detournay 1999) . So in the viscosity-dominated regime, the solution is independent of the toughness K', while in the toughness-dominated regime the solution is independent of the viscosity μ'.

An important restriction of the analysis reported here stems from the assumption that the fracture remains parallel to the free-surface. In fact, the fracture will eventually curve towards the free-surface as the mode II stress intensity factor K_{II} is non-zero for a planar fracture if $\mathcal{R} = R/H > 0$. However, the solutions developed here is valid in the asymptotic sense when the main parameter controlling the curving of the fracture, $\chi = K_{\rm Ic}/\sigma_o\sqrt{H}$ (if $\alpha = 0$), is small (Detournay et al. 2001).

The paper is organized as follows. First, we describe the mathematical formulation of this problem, in particular the elasticity component which is based on singular integral equations. Next, we reformulate the equations using a viscosity-scaling appropriate for "small" toughness and a toughness-scaling for "small" viscosity. Then we construct the zero-toughness and large toughness asymptotic solutions, and conclude with a presentation of an example from inducing caving at Moonee Colliery.

2 PROBLEM FORMULATION

2.1 *Elasticity*

A non-local elasticity relation exists between the fracture opening $w(r,t)$ and the net pressure $p(r,t)$. By reference to Fig. 1, it is convenient to introduce the normal and shear displacement discontinuities, D_n and D_s, which correspond here to

$$D_n = [u_z] = u_z^+ - u_z^- \quad (2)$$

$$D_s = [u_r] = u_r^+ - u_r^- \quad (3)$$

where the superscript $+$ and $-$ refers to the upper and lower surface of the fracture, respectively. Obviously, the fracture opening w is equal to the normal displacement discontinuity D_n. The lack of opening symmetry caused by the presence of a free surface is responsible for the existence of a shear displacement discontinuity D_s.

Using the singular solutions for displacement discontinuity loops, two singular integral equations can be established

$$\int_0^R G_{nn}\left(\frac{r}{R},\frac{s}{R};\mathcal{R}\right) D_n(s,t)ds + \int_0^R G_{ns}\left(\frac{r}{R},\frac{s}{R};\mathcal{R}\right) D_s(s,t)ds = -\frac{R^2}{E'}p(r,t) \quad (4)$$

$$\int_0^R G_{sn}\left(\frac{r}{R},\frac{s}{R};\mathcal{R}\right) D_n(s,t)ds + \int_0^R G_{ss}\left(\frac{r}{R},\frac{s}{R};\mathcal{R}\right) D_s(s,t)ds = 0 \quad (5)$$

The first equation simply expresses that the normal stress across the fracture plane, induced by a distribution of normal and shear displacement discontinuities is equal to the net pressure (to a minus sign), while the second equation satisfies the condition of zero shear stress on the fracture wall. The influence functions $G's$ are hypersingular as they contain the strong singularity $(r-s)^{-2}$; also they depend only on the geometric parameter $\mathcal{R} = R/H$, but not on the elastic constants of the half-space, see Zhang et al. (2000) for details. Note that the dependence of D_n and D_s on time t is strictly via the loading $p(r,t)$.

In principle, (5) can be inverted to yield

$$D_s = \mathcal{F}\{D_n;\mathcal{R}\} \quad (6)$$

where $\mathcal{F}$ is a linear operator. In view of (6), the first integral equation (4) can thus be rewritten as

$$\mathcal{H}\left\{\frac{w}{R};\mathcal{R}\right\} = \frac{p}{E'} \quad (7)$$

where $\mathcal{H}$ is linear functional (also, w has been substituted to D_n). Equation (7) expresses the non-local relationship between the fracture opening w and the net pressure p.

There are two numerical methods to solve these integral equations: the displacement discontinuity method (DDM) to solve (4)-(5) based on approximating the continuous function $w = D_n$ by a piecewise constant function, and the Chebyshev polynomial method (CPM) due to Erdogan et al (1973) based on approximating the regular function $h_n(r)$

$$h_n = \left(\frac{R-r}{R+r}\right)^{1/2} d_n(r) \tag{8}$$

in which d_n is the slope of discontinuities, by a truncated series of orthogonal polynomials. The first method is more flexible (it is used in conjunction with the lubrication equation), but the second provides more accurate results for the same number of degrees of freedom, in particular in the evaluation of the stress intensity factors K_{I} and K_{II}.

2.2 *Lubrication*

The equation governing the flow of viscous fluid in the fracture is the non-linear Reynolds differential equation from lubrication theory

$$\frac{\partial w}{\partial t} = \frac{1}{\mu' r}\frac{\partial}{\partial r}\left(r w^3 \frac{\partial p}{\partial r}\right) \tag{9}$$

which is obtained by eliminating the flow rate q between Poiseuille law

$$q = -\frac{w^3}{\mu'}\frac{\partial p}{\partial r} \tag{10}$$

and the continuity equation for an impermeable solid

$$\frac{\partial w}{\partial t} + \frac{1}{r}\frac{\partial (rq)}{\partial r} = 0 \tag{11}$$

In this analysis, the fracture is completely filled by the fracturing fluid, i.e. there is no lag between the fluid front and the fracture tip. This assumption is responsible for the existence of a singularity in the fluid pressure at the tip of the propagating fracture. For an impermeable elastic solid with zero toughness, the fluid pressure is characterized by a cube root singularity (Desroches et al. 1994) . The cube root singularity can be understood as an intermediate asymptote, which reflects in general a situation where the energy expended in the creation of new fracture surfaces is small compared to the energy dissipated in viscous flow (Detournay,1999) .

2.3 *Boundary Conditions and Initial Conditions*

The problem is completely formulated with the addition of a propagation criterion and boundary conditions at the fracture inlet $r = 0$ and at the tip $r = R(t)$. The condition that the fracture is in mobile equilibrium, $K_I = K_{Ic}$, can be expressed as

$$w \simeq \frac{K'}{E'}(R-r)^{1/2} \qquad R - r \ll R \tag{12}$$

Besides the condition $w(R,t) = 0$ which is obviously implied by the opening asymptote (12), the boundary conditions consist of

$$q(R,t) = 0 \quad \text{and} \quad 2\pi \lim_{r\to 0} rq = Q_o \tag{13}$$

It follows from the above equation, that $q \sim O(1/r)$ near the source and thus that $p \sim -\ln r$. Alternatively, the source can be taken into account by the global continuity equation

$$2\pi \int_0^R r\, w \mathrm{d}r = Q_o t \tag{14}$$

The initial conditions for this problem are actually given by the solution for the full-space, as we do not analyze the early episode of the fracture life when it initiates and propagates from the wellbore. By disregarding fracture initiation from the wellbore, the depth H is the only characteristic length entering the description of this problem. Hence, the initial conditions correspond in the limit $\mathcal{R} = 0$, i.e. to the solution of a penny-shaped fracture in full-space. For the two limiting solutions considered in this analysis, the zero-toughness and the zero-viscosity solutions, the initial solutions $\mathcal{R} = 0$ are in fact self-similar and are characterized by a power law dependence on time t (Savitski & Detournay, 2001).

3 SCALING AND TWO LIMITING SOLUTIONS

3.1 *Solution of diffusion equation*

The scaling method follows Detournay(2001) and Savitski & Detournay (2001) for the case $\mathcal{R} = 0$. First, we express the crack opening $w(r,t)$ and the net pressure $p(r,t)$ as

$$w = \varepsilon(t) L(t) \Omega(\rho, \mathcal{R}) \quad p = \varepsilon(t) E' \Pi(\rho, \mathcal{R}) \tag{15}$$

where the scaled opening Ω and pressure Π are function of the spatial coordinate $\rho = r/R(t)$ and the evolution parameter $\mathcal{R}$, both dimensionless variables. Furthermore, $\varepsilon(t)$ is a small dimensionless parameter and $L(t)$ a length scale of the same order as the fracture radius $R(t)$. The two lengths $R(t)$ and $L(t)$ are related by

$$R(t) = \gamma(\mathcal{R}) L(t) \tag{16}$$

where the length factor γ is defined by

$$2\pi \gamma^2 \int_0^1 \rho \Omega d\rho = 1 \tag{17}$$

The governing equations can readily be rewritten in terms of the new variables, after noting that the derivative terms in the lubrication equation (9) can be expressed in terms of ρ and $\mathcal{R}$

$$\left.\frac{\partial}{\partial r}\right|_t = \frac{1}{R}\frac{\partial}{\partial \rho}, \qquad \left.\frac{\partial}{\partial t}\right|_r = \dot{\mathcal{R}}\,(\quad)' - \rho\frac{\dot{\mathcal{R}}}{\mathcal{R}}\frac{\partial}{\partial \rho} \tag{18}$$

where the prime denotes differentiation with respect to $\mathcal{R}$, and the dot differentiation with respect to t. Hence,

- elasticity

$$\Pi = \gamma^{-1}\mathcal{H}\left\{\Omega; \mathcal{R}\right\} = \mathcal{H}\left\{\Omega/\gamma\,; \mathcal{R}\right\} \tag{19}$$

- lubrication

$$\begin{aligned}\left(\frac{\dot{\varepsilon}t}{\varepsilon} + \frac{\dot{L}t}{L}\right)\Omega + \dot{\mathcal{R}}t\Omega' - \rho\frac{\dot{\mathcal{R}}t}{\mathcal{R}}\frac{\partial \Omega}{\partial \rho} \\ = \quad \frac{1}{\gamma^2\rho}\frac{\partial}{\partial \rho}\left(\rho\Omega^3\frac{\partial \Pi}{\partial \rho}\right)\end{aligned} \tag{20}$$

- global fluid volume balance

$$\varepsilon L^3 = Q_o t \tag{21}$$

- propagation criterion

$$\Omega = \frac{K'}{\varepsilon E' L^{1/2}}\gamma^{1/2}\,(1-\rho)^{1/2} \quad 1-\rho \ll 1 \tag{22}$$

Consider now the viscosity-scaling, denoted by the subscript μ. The small parameter ε_μ is deduced by imposing that the viscosity does not appear in the lubrication equation (20). The explicit dependence of the length scale L_μ on time t then follows from the global mass balance (21). Hence,

$$\varepsilon_\mu = \left(\frac{\mu'}{E't}\right)^{1/3}, \quad L_\mu = \left(\frac{E' Q_o^3 t^4}{\mu'}\right)^{1/9} \tag{23}$$

The lubrication equation simplifies therefore to

$$\frac{1}{9}\Omega_{\mu 0} + \dot{R}t\Omega'_\mu - \rho\frac{\dot{\mathcal{R}}t}{\mathcal{R}}\frac{\partial \Omega_\mu}{\partial \rho} = \frac{1}{\gamma_\mu^2\rho}\frac{\partial}{\partial \rho}\left(\rho\Omega_\mu^3\frac{\partial \Pi_\mu}{\partial \rho}\right) \tag{24}$$

The dimensionless toughness $\mathcal{K}(t)$ can now be defined as

$$\mathcal{K} = K'\left(\frac{t^2}{\mu'^5\, Q_o^3 E'^{13}}\right)^{1/18} \tag{25}$$

so that the propagation criterion in terms of the opening tip asymptote (22) becomes

$$\Omega_\mu = \mathcal{K}\gamma_\mu^{1/2}\,(1-\rho)^{1/2}, \quad 1-\rho \ll 1 \tag{26}$$

In the toughness-scaling (denoted by the subscript κ), the small parameter ε_κ is defined by requiring that there are no toughness parameters left in the propagation criterion (22)

$$\Omega_\kappa = \gamma_\kappa^{1/2}\,(1-\rho)^{1/2}, \quad 1-\rho \ll 1 \tag{27}$$

Taking into account the fluid mass balance (21) yields the explicit power law dependence of both ε_κ and L_κ on time t

$$\varepsilon_\kappa = \left(\frac{K'^6}{E'^6 Q_o t}\right)^{1/5}, \; L_\kappa = \left(\frac{Q_o^2 E'^2 t^2}{K'^2}\right)^{1/5} \tag{28}$$

It is also natural to introduce a dimensionless viscosity $\mathcal{M}(t)$

$$\mathcal{M} = \mu'\left(\frac{Q_o^3 E'^{13}}{K'^{18} t^2}\right)^{1/5} \tag{29}$$

so that the lubrication equation (20) can now be rewritten as

$$\begin{aligned}\mathcal{M}\left(\frac{1}{5}\Omega_\kappa + \dot{\mathcal{R}}t\Omega'_\kappa - \rho\frac{\dot{\mathcal{R}}t}{\mathcal{R}}\frac{\partial \Omega_\kappa}{\partial \rho}\right) \\ = \quad \frac{1}{\gamma_\kappa^2\rho}\frac{\partial}{\partial \rho}\left(\rho\Omega_\kappa^3\frac{\partial \Pi_\kappa}{\partial \rho}\right)\end{aligned} \tag{30}$$

3.2 *Zero-Toughness solution ($K = 0$)*

We first discuss the construction of the zero-toughness solution $\mathcal{F}_{\mu 0}(\rho, \mathcal{R}) = \{\Omega_{\mu 0}, \Pi_{\mu 0}, \gamma_{\mu 0}\}$. (The subscript 0 following μ is used to refer to the limiting case $\mathcal{K} = 0$.) The equations governing the quantities $\Omega_{\mu 0}$, $\Pi_{\mu 0}$, $\gamma_{\mu 0}$ (i.e. elasticity, lubrication, propagation criterion, and volume balance) are specialized versions of (19), (24), (22), and (17), respectively

$$\mathcal{H}\left\{\Omega_{\mu 0}/\gamma_{\mu 0}; \mathcal{R}\right\} = \Pi_{\mu 0} \tag{31}$$

$$\begin{aligned}\Omega_{\mu 0} + \frac{4\gamma_{\mu 0}\mathcal{R}}{\gamma_{\mu 0} - \gamma'_{\mu 0}\mathcal{R}}\Omega'_{\mu 0} - \frac{4\gamma_{\mu 0}\rho}{\gamma_{\mu 0} - \gamma'_{\mu 0}\mathcal{R}}\frac{\partial \Omega_{\mu 0}}{\partial \rho} \\ = \frac{9}{\gamma_{\mu 0}^2\rho}\frac{\partial}{\partial \rho}\left(\rho\Omega_{\mu 0}^3\frac{\partial \Pi_{\mu 0}}{\partial \rho}\right)\end{aligned} \tag{32}$$

$$\lim_{\rho \to 1}(1-\rho)^{-1/2}\,\Omega_{\mu 0} = 0 \tag{33}$$

$$2\pi\gamma_{\mu 0}^2\int_0^1 \rho\Omega_{\mu 0}\,d\rho = 1 \tag{34}$$

The particular form (32) of the lubrication equation makes use of the following expression for the term $\dot{\mathcal{R}}t$ in (24)

$$\dot{\mathcal{R}}t = \frac{4\gamma_{\mu 0}\mathcal{R}}{9\left(\gamma_{\mu 0} - \gamma'_{\mu 0}\mathcal{R}\right)} \tag{35}$$

which is obtained by differentiating $\mathcal{R}(t) = \frac{\gamma_{\mu 0}(\mathcal{R}) L_\mu(t)}{H}$ with respect to time t.

Together, (31)-(33) imply that the near-tip behavior of the solution as given by Desroches et al. (1994)

$$\Omega_{\mu 0} \sim (1-\rho)^{2/3} \quad \Pi_{\mu 0} \simeq -(1-\rho)^{-1/3} \tag{36}$$

It must be emphasized that the above asymptotic behavior is built on the assumption that the fluid front coincides with the fracture tip.

The solution $\mathcal{F}_{\mu 0}$ of the system of equations (31)-(34) does not depend on any parameters, other than the independent variables $(\rho, \mathcal{R})$. The solution $\mathcal{F}_{\mu 0}$ can be obtained by solving an evolution problem in $\mathcal{R}$, starting with the known self-similar solution at $\mathcal{R} = 0$ (Savitski & Detournay, 2001). We choose to solve this problem by modeling numerically the propagation of a penny-shaped fracture on a fixed-grid. This approach takes advantage of an algorithm originally devised by Savitski (2000) for the case $\mathcal{R} = 0$, which is based on the displacement discontinuity method to solve the elasticity equation (31), and on an implicit finite difference scheme to solve the lubrication equation (32), see Savitski (2000) for details. The solution for different $\mathcal{R}$ is characterized by increasing accuracy with 125 nodes grows linearly with $\mathcal{R}$ on a fixed grid.

Once the function $\gamma_{\mu o}(\mathcal{R})$ has been determined numerically, the dependence of $\mathcal{R}$ on t is deduced by solving the implicit equation

$$\frac{\mathcal{R}}{\gamma_{\mu 0}(\mathcal{R})} = \frac{1}{H}\left(\frac{E' Q_o^3 t^4}{\mu'}\right)^{1/9} \tag{37}$$

which is derived from $R(t) = \gamma_{\mu o}(\mathcal{R}) L_\mu(t)$ and the definition $\mathcal{R} = R/H$.

3.3 *Zero-Viscosity solution ($M = 0$)*

We now focus on computing the zero-viscosity solution $\mathcal{F}_{\kappa 0} = \{\Omega_{\kappa 0}, \Pi_{\kappa 0}, \gamma_{\kappa 0}\}$, where the subscript 0 following κ is here used to refer to the limiting case for $\mathcal{M} = 0$. The solution $\mathcal{F}_{\kappa 0}$, like $\mathcal{F}_{\mu 0}$, does not depend on any parameters other than $(\rho, \mathcal{R})$. For this limiting case, the lubrication equation (30) degenerates into

$$\rho \Omega_{\kappa 0}^3 \Pi'_{\kappa 0} = 0 \tag{38}$$

which indicates that the net pressure $\Pi_{\kappa 0}$ is uniform; hence $\Pi_{\kappa 0} = \Pi_{\kappa 0}(\mathcal{R})$. The set of governing equations simplify therefore to

$$\mathcal{H}\left\{\bar{\Omega}_{\kappa 0}; \mathcal{R}\right\} = \Pi_{\kappa 0} \tag{39}$$

$$2\pi \gamma_{\kappa 0}^3 \int_0^1 \rho \bar{\Omega}_{\kappa 0} d\rho = 1 \tag{40}$$

$$\lim_{\rho \to 1} (1-\rho)^{-1/2} \gamma_{\kappa 0}^{1/2} \bar{\Omega}_{\kappa 0} = 1 \tag{41}$$

where it was found convenient to define $\bar{\Omega}_{\kappa 0} = \frac{\Omega_{\kappa 0}}{\gamma_{\kappa 0}}$. The method used to calculate the solution $\mathcal{F}_{\kappa 0}(\rho, \mathcal{R})$ takes advantage of the linearity of the governing equations when $\mathcal{M} = 0$. Thus, we introduce the crack opening $\Omega_*(\rho; \mathcal{R})$ corresponding to a unit pressure in the fracture, i.e., $\mathcal{H}\{\Omega_*; \mathcal{R}\} = 1$, and the corresponding length factor $\gamma_*(\mathcal{R})$

$$2\pi \gamma_*^3 \int_0^1 \rho \Omega_* d\rho = 1 \tag{42}$$

Also, we define the stress intensity factor $K_*(\mathcal{R})$ such that $\Omega_* \simeq K_* (1-\rho)^{1/2}$ near the tip $\rho = 1$. It follows from these definitions that

$$\bar{\Omega}_{\kappa 0} = \Pi_{\kappa 0}(\mathcal{R}) \Omega_*(\rho; \mathcal{R}), \quad \gamma_{\kappa 0} = \Pi_{\kappa 0}^{-1/3} \gamma_* \tag{43}$$

Finally, the net pressure $\Pi_{\kappa 0}(\mathcal{R})$ is computed from the propagation criterion (41), by substituting $\bar{\Omega}_{\kappa 0}$ and $\gamma_{\kappa 0}$ in (43)

$$\Pi_{\kappa 0} = \left(\gamma_* K_*^2\right)^{-3/5} \tag{44}$$

It then follows that

$$\gamma_{\kappa 0} = \left(\gamma_*^3 K_*\right)^{2/5} \quad \Omega_{\kappa 0} = \left(\gamma_*^3 K_*^{-4}\right)^{1/5} \Omega_*(\rho) \tag{45}$$

Calculation of the crack aperture Ω_* is carried out using either the Chebyshev polynomial method (Erdogan et al. 1973) or the displacement discontinuity method (Crouch & Starfield, 1983). The shape factor γ_* is then computed according to (42) and the stress intensity factor K_* from the asymptotics of Ω_*. Once the function $\gamma_{\kappa 0}(\mathcal{R})$ has been determined, the dependence of $\mathcal{R}$ on t is deduced in the same way as zero-toughness cases. Note finally that the solution $\mathcal{F}_{\kappa 0}$ in the limit $\mathcal{R} = 0$ is given by Savitski (2000)

$$\begin{aligned} \Omega_{\kappa 0} &= \left(\frac{3}{2^3 \pi}\right)^{1/5} (1-\rho^2)^{1/2} \\ \Pi_{\kappa 0} &= \left(\frac{\pi^6}{2^{17} 3}\right)^{1/5} \quad \gamma_{\kappa 0} = \left(\frac{3^2}{2\pi^2}\right)^{1/5} \end{aligned} \tag{46}$$

4 RESULTS FOR NORMALIZED PARAMETERS

The variation with $\mathcal{R}$ of the volumetric factors $\gamma_{\mu 0}(\mathcal{R})$ and $\gamma_{\kappa 0}(\mathcal{R})$, maximum opening $\Omega_{\mu o}(0, \mathcal{R})$ and $\Omega_{\kappa o}(0, \mathcal{R})$ and net pressure $\Pi_{\kappa o}(\mathcal{R})$ is illustrated in Figs 2-4. These figures show not only the numerical results for specific values of $\mathcal{R}$ but also the best-fit polynomials $F(\mathcal{R}) = \sum_{i=0}^{i=n} a_i \mathcal{R}^i$ that can be used to interpolate the results. The coefficients a_i of the best-fit polynomials can be found in Table 1. Figures 2-3 indicate that with increasing $\mathcal{R}$ the fracture become shorter and wider, in relative terms compared to the deep crack solution ($\mathcal{R} = 0$). Figure 4 shows that a smaller pressure, compared to the case $\mathcal{R} = 0$ is required to drive the fracture in the zero-viscosity limit.

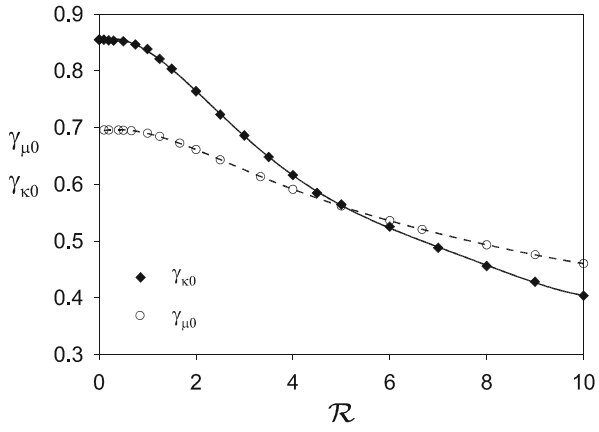

Figure 2: Variation of volumetric factor $\gamma_{\mu o}$ and $\gamma_{\kappa o}$ with R. The symbols correspond to numerical results, and the curves to a best-fit polynomial

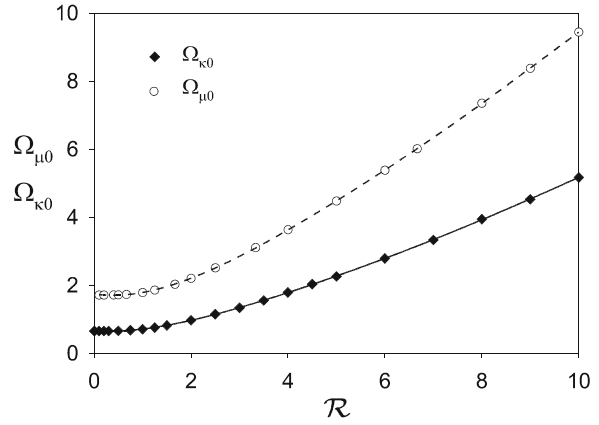

Figure 3: Variation of opening $\Omega_{\mu o}$ and $\Omega_{\kappa o}$ at the fracture center with R. The symbols correspond to numerical results, and the curves to a best-fit polynomial

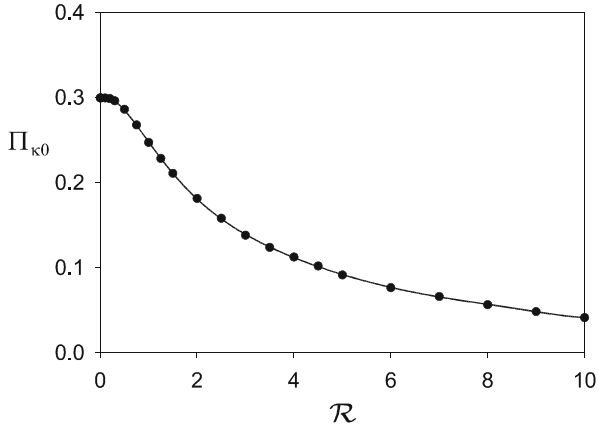

Figure 4: Variation of the uniform pressure $\Pi_{\kappa o}$ with R. The symbols correspond to numerical results, and the curve to a best-fit polynomial

Table 1: Coefficients of fitting curves for non-dimensional parameters

	$\gamma_{\kappa o}$	$\Pi_{\kappa o}$	$\Omega_{\kappa o}$	$\gamma_{\mu o}$	$\Omega_{\mu o}$
a_0	0.852	0.299	0.659	0.693	1.740
$a_1 \cdot 10^1$	0.297	0.272	-0.912	0.174	-2.014
$a_2 \cdot 10^1$	-0.610	-0.156	0.1675	-0.266	2.836
$a_3 \cdot 10^2$	1.509	11.34	-2.741	0.623	-3.843
$a_4 \cdot 10^3$	-1.649	-44.87	2.671	-0.708	2.582
$a_5 \cdot 10^5$	8.078	1124	-13.09	4.008	-4.006
$a_6 \cdot 10^6$	-1.323	-1860	2.392	-0.896	-2.045
$a_7 \cdot 10^4$		2.033			
$a_8 \cdot 10^5$		-1.409			
$a_9 \cdot 10^7$		5.611			
$a_{10} \cdot 10^9$		-9.752			

Table 2: Coefficients of the best-fit polynomials for $\Pi^1_{\mu o}$, $\Pi^2_{\mu o}$, and $\Pi^3_{\mu o}$

	$\Pi^1_{\mu o}$	$\Pi^2_{\mu o}$	$\Pi^3_{\mu o}$
a_0	0.74052	0.98882	0.87424
a_1	0.95563	0.62105	0.89508
a_2	−1.45075	−1.1842	−1.49911
a_3	0.89298	0.73728	0.93627
a_4	−0.33648	−0.26871	−0.34275
$a_5 \cdot 10^2$	8.50119	6.39297	8.0854
$a_6 \cdot 10^2$	−1.46577	−1.01733	−1.25927
$a_7 \cdot 10^3$	1.6963	1.06972	1.284157
$a_8 \cdot 10^4$	−1.2556	−0.71034	−0.82323
$a_9 \cdot 10^6$	5.3535	2.68703	3.0052
$a_{10} \cdot 10^8$	−9.9755	−4.3944	−4.7584

5 APPLICATIONS

The evolution with time of the fracture radius, maximum crack opening, and pressure at the wellbore can be determined for specific parameters, simply by scaling the theoretical solutions derived for the viscosity-dominated and toughness-dominated regime of solution. There is a difficulty, however, in predicting the wellbore pressure for the zero-viscosity solution, not only because the fixed well radius a corresponds to varying $\rho = a/R(t)$ as the fracture propagates, but also because of the logarithmic singularity of the pressure at the center. In contrast, the opening is nearly constant for $\rho < 0.05$ and it is therefore legitimate to adopt $\Omega(0)$ for the fracture opening at the well as long as $a/R(t) \leq 0.05$.

As a pragmatic solution, the pressure at the well is interpolated from $\Pi_{\mu 0}(\alpha, \mathcal{R})$ evaluated at $\alpha = 0.01$, 0.00278 and 0.001. (These three functions, denoted respectively as $\Pi^1_{\mu o}$, $\Pi^2_{\mu o}$, and $\Pi^3_{\mu o}$ are plotted in Fig. 5 with the coefficients of the best-fit polynomials listed in Table 2.

As an example consider the following parameters: $E = 20$ GPa, $\nu = 0.28$ (giving $E' = 21.7$ GPa), $K_{Ic} = 1.5$ MPa$\sqrt{\text{m}}$; $H = 9$ m; $Q_o = 0.360$ m^3/min,

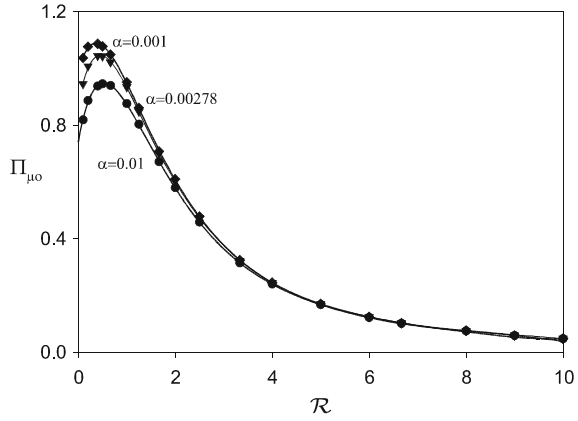

Figure 5: Plot of $\Pi_{\mu o}$ vs R for the zero-toughness cases. The scatter points are adopted from the DDM results and the solid line is the fitting curve.

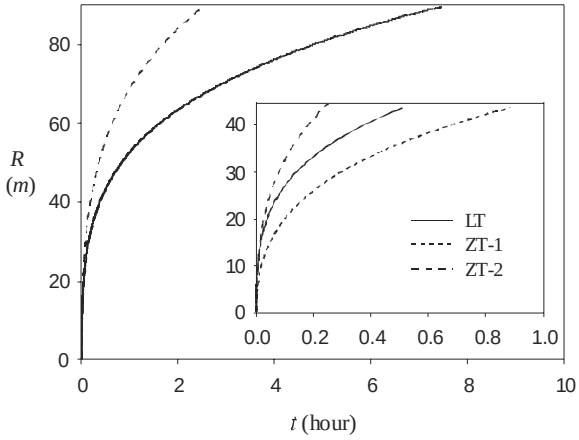

Figure 6: Variation of the fracture radius R with time for the two viscosity cases: $\mu = 0.2$ Pa·s (small dash) and $\mu = 0.001$ Pa·s (long dash).

$\mu = 0.2, 0.001$ Pa·s (high and low viscosity fracturing fluid referred to as ZT-1 and ZT-2, respectively, on the following plots). The radius of the borehole is 25 mm (this is used to calculate the inlet pressure). Evolution of the fracture radius, as well as the net pressure and the fracture opening at the well are show in Figs. 6, 7 and 8 for both the zero-viscosity and zero-toughness bounds. The effect of the fluid viscosity on the zero-toughness solution can be observed in these figures. At any given time, the high viscosity case is characterized by a smaller fracture radius, but a larger net pressure and wider opening compared to the low viscosity case.

6 CONCLUSIONS

In this paper, we have derived two asymptotic solutions for a penny-shaped hydraulic fracture propagating parallel to the free-surface of an elastic half-space. The fracture is driven by an incompressible Newtonian fluid injected at a constant rate at the center of the fracture. The two limiting solutions are constructed

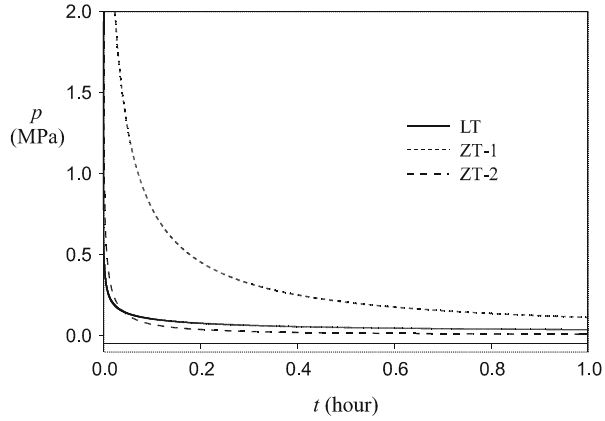

Figure 7: Variation of the net pressure with time for the two viscosity cases: $\mu = 0.2$ Pa·s (small dash) and $\mu = 0.001$ Pa·s (long dash).

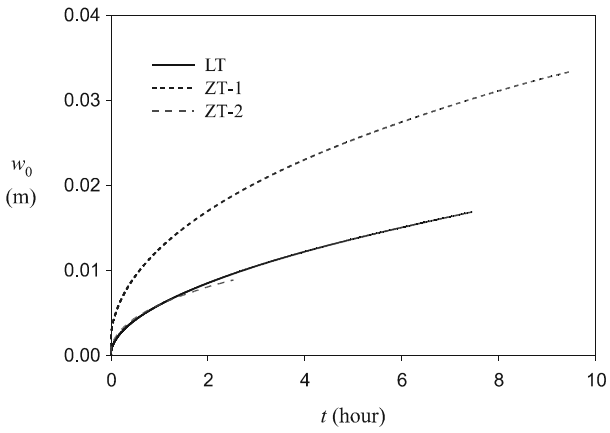

Figure 8: Variation of the fracture opening at the well with time, for the two viscosity cases: $\mu = 0.2$ Pa·s (small dash) and $\mu = 0.001$ Pa·s (long dash).

on the assumption that either the solid has no toughness or that the fluid has no viscosity. One important outcome of the analysis is demonstrating that the asymptotic solutions depend only on the dimensionless parameter $\mathcal{R}$, when properly scaled. The scaled solution can thus be tabulated once and for all. The dependence of the solution on time can be retrieved for specific parameters, through simple scaling and by solving an implicit equation such as $\mathcal{L}_{\mu 0}(t)\gamma_{\mu 0}(\mathcal{R}) = \mathcal{R}$ for the zero toughness case (and a similar one for the zero viscosity case).

One specific case is studied with material parameters and geometry similar to real caving events at Moonee, but without considering fluid loss which is known to be important in this application. The variations of the crack radius, the inlet pressure and the crack opening are presented. The varing trends with time in crack radius amd pressure are consistent in trend with the measured ones *in situ*. Detailed comparison between theoretical prediction and experimental observations are given by Jeffrey et al. (2001).

7 REFERENCES

Crouch, S.L. & Starfield, A.M. 1983. *Boundary Element Methods in Solid Mechanics*. George Allen & Unwin.

Desroches, J., Detournay, E., Lenoach, B., Papanastasiou, J.R., Pearson, J.R.A., Thiercelin, M. & Cheng, A.H-D 1994. The crack tip region in hydraulic fracturing. *Proc. Roy. Soc. London (A)* A447: 39-48.

Detournay, E. 1999. Fluid and solid singularities at the tip of a fluid-driven fracture. In D. Durban & J.R.A. Pearson (eds), *Nin-Linear Singularities in Deformation and Flow*, 27-42, Dordrecht: Kluwer.

Detournay, E. 2001. Propagation regimes of fluid-driven fractures in impermeable rocks. In C. Desai (ed.) *Proc. Int. Conf. On Computer Methods and Advances in Geomechanics*, Rooterdam: Balkema.

Detournay, E., Zhang, X. & Jeffrey, R. G. 2001. Influence of a free-surface on the propagation of a hydraulic fracture. *Int. J. Rock Mech. Min. Sci.* in preparation.

Erdogan, F., Gupta, G.D. & Cook, T.S. 1973. Numerical solution of singular integral equations. *Mechanics of Fracture* vol. 1, 368-425. Noordhoff International Publishing.

Jeffrey, R.G. & Settari, A. 2000. Hydraulic fracturing growth through offset pressure-monitoring wells and boreholes. In *The SPE Annual Tech. Conf. and Exhib. SPE 63031*. Dallas.

Jeffrey, R. G. & Mills, K.W. 2000. Hydraulic fracturing applied to inducing longwall coal mine goaf falls. In *Pacific Rocks 2000*. 423-430. Seattle. Balkema.

Jeffrey, R.G., Settari, A., Mills, K.W., Zhang, X. & Detournay, E. 2001. Hydraulic fracturing to induce caving: Fracture model development and comparison to field data. *In DC Rocks*. Washington, DC.

Pollard, D.D. & Hozhausen, G. 1979. On the mechanical interaction between a fluid-filled fracture and the earth's surface. *Tectonophysics* 53: 27-57.

Savitski, A. 2000. Propagation of a penny-shaped hydraulic fracture in an impermeable rock. *Ph.D. Thesis*, University of Minnesota.

Savitski, A. & Detournay, E. 2000. Similarity solution of a penny-shaped fluid-driven fracture in a zero-toughness linear elastic solid. *C. R. Acad. Sc. Paris*, submitted.

Wang. G., Dusseault, M.B., Pindera, J.T. & Rothenburg, L. 1994. Influence of subsurface fractures on surface deformation of an elastic half-space. *Int. J. Numer. Anal. methods Geomech*. 18: 287-303.

Zhang, X., Detournay, E. & Jeffrey, R.G. 2000. Propagation of a penny-shaped hydraulic fracture parallei to the free-surface of an elastic half-space. *Technical Report* 00-036, CSIRO Petroleum, Melbourne.